

FILM DEPOSITION, CRYOGENIC RF TESTING AND MATERIALS ANALYSIS OF A Nb/Cu SINGLE CELL SRF CAVITY *

X. Zhao[#], R.-L. Geng, Y. Li, A.D. Palczewski

Thomas Jefferson National Accelerator Facility, Newport News, Virginia 23606

Abstract

In this study, we present preliminary results on using a cathodic-arc-discharge Nb plasma ion source to establish a Nb film-coated single-cell Cu cavity for SRF research. The polycrystalline Cu cavity was fabricated and mirror-surface-finished by a centrifugal barrel polishing (CBP) process at Jefferson Lab. Special pre-coating processes were conducted, in order to create a template-layer for follow-on Nb grain thickening. A sequence of cryogenic RF testing demonstrated that the Nb film does show superconductivity. But the quality factor of this Nb/Cu cavity is low as a result of high residual surface resistance. We are conducting a thorough materials characterization to explore if some microstructural defects or hydrogen impurities, led to such a low quality factor.

INTRODUCTION

The mainstream superconducting resonators are fabricated using high-purity bulk niobium material. Due to the high material cost, the bulk niobium technology becomes less favorable when large number of resonators or large sized resonators are required. An alternative technology is to coat the inner surface of a copper resonator with a thin layer (typically on the order of a few microns) of superconducting niobium. As the functioning superconducting layer is characterized by the London penetration depth (which is on the order of few tens of nanometers for niobium), the coated thin layer is fully capable of supporting the required super-current. As compared to the bulk niobium technology, which requires typically a few millimeters wall thickness, the coated thin film niobium technology offers a significant saving in material cost for fabrication of superconducting resonators. In addition, the thermal conductivity of copper at cryogenic temperatures is superior to that of the niobium, rendering improved thermal stability for operation of the superconducting resonators in practical applications. Another advantage of niobium coated thin film technology lies in the fact resonators thus fabricated have been far less sensitive to the ambient magnetic field as compared to the bulk technology. This effect leads to the simplification to the design and realization of magnetic shielding for the resonators and therefore further saves the cost of the cryomodules that host the superconducting resonators.

Thin film niobium coated copper cavity technology was previously realized by using the magnetron sputtering technique. Despite some successful applications, the sputtered Nb-Cu technology has not found applications in

regime of acceleration gradients higher than 10 MV/m. This is due to a problem of rapid increase of surface losses as the gradient is raised.

The method of making Nb-Cu resonators described in this study is characterized by several novel aspects which aimed to yield improved properties of the final functioning superconducting surface.

METHODS

Our goal is to create a multiple-layer structure of Nb film for SRF application. Our microstructure design of the film has such novelty: I. It contains a Template-Layer between underlying copper substrate and a thickening layer made of Nb material; II. The Template-Layer, being established by a post-energetic-condensation thermodynamic nucleation process, can yield controllable grains (crystal) size/distribution; III. The Nb grains in the Thickening-Layer have a polycrystalline fibrous structure, whose texture is gauged by the aforementioned Template-Layer.

Our proposed growth mode is different than epitaxial growth of Nb film on a polycrystalline Cu substrate, in which the grain size and distribution of Nb grains are gauged by underlying copper grains. One potential advantage of this microstructure design is to avoid complicated finishing process (which would be required by a Nb-Cu epitaxy), and is able to tune Nb microstructure (grain size, distribution, grain boundaries characters) in order to optimize an SRF surface layer.

Fig. 1 schematically illustrates one sample of our conceptual design of this multi-layer Nb film (in a cross-section view). The microstructure has four layers: a Buffer Layer (Layer X), a Template Layer, a Thickening Layer and an SRF function / Surface Layer. The Template Layer, Thickening Layer and Surface Layer are made of pure niobium. Composition of the Buffer Layer can be one of, but not limited to, such choices: magnesium oxide, aluminium oxide, silicon oxide, copper oxide, niobium oxide, aluminium nitride. The Buffer Layer can be of either amorphous or polycrystalline structure.

To conduct the coating work, a single-cell SRF cavity made of a commercial OFHC copper was fabricated at Jefferson Lab. Its structure design has a *low surface field* (LSF) shape. Dimensions of the cavity (called LSF1-1) are shown in Fig. 2.

*Work supported by Jefferson Science Associates, LLC under U.S. DOE Contract No. DE-AC05-06OR23177.

[#]xinzhao@jlab.org

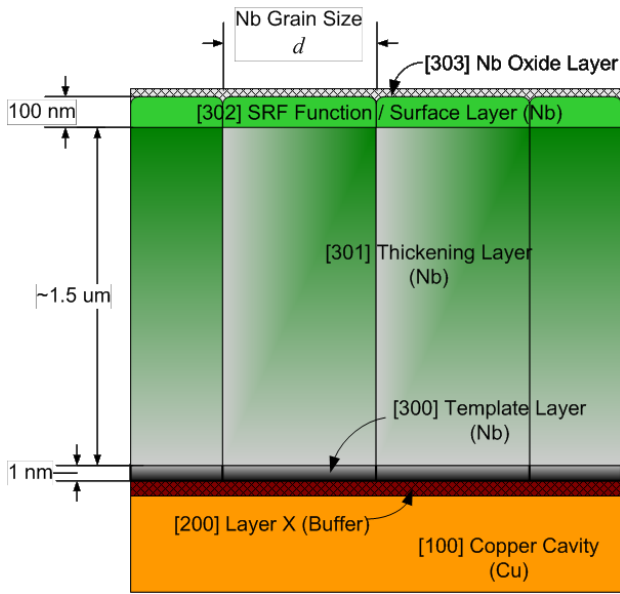


Fig. 1: A conceptual illustration of microstructure design of a multi-layer Nb film coating for SRF cavity.

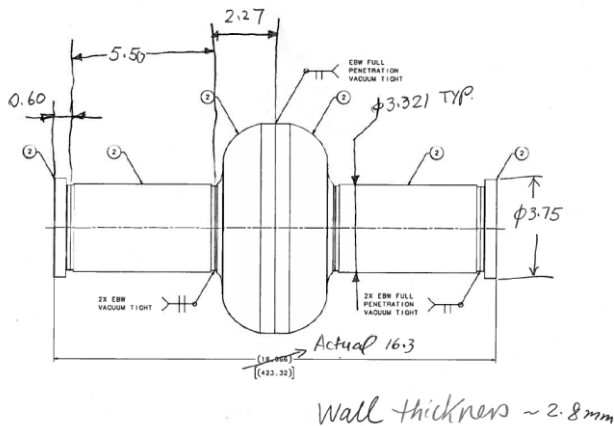


Figure 2: LSF1-1 cavity model and key dimensions. Cavity ID at equator: 7.814 inch typical; Cavity OD at equator: 7.940 typical; Beam tube ID: 3.07 typically.

The cavity half cells and beam pipes were welded together by a standard EBW procedure. After welding, the cavity did not receive any chemistry or cleaning prior to a centrifugal barrel polishing (CBP) [1]. After CBP, the LSF1-1 cavity was cleaned by a standard high pressure rinse (HPR) procedure. There was no chemical treatment following CBP. The LSF1-1 was sent to AASC Company for Nb film deposition. AASC's deposition method, coaxial energetic condensation (CED) has been described elsewhere [2]. The energetic condensation was conducted via a cathodic arc-discharge Nb ion deposition. Such Nb plasma deposition uses a low voltage (30 V) arc discharge to generate a highly ionized plasma. The energy spectrum of ions from coaxial energetic deposition (CED) ranges from 20 eV to 170 eV.

Besides using AASC's CED coating technology, a novel contribution of this work was implementing our special procedure to embody our multilayer microstructure design:

1. Pumping down the LSF1-1 cavity for 3hr after mounting the cavity into AASC CED Coater facility.
2. Baking the cavity at 150°C ($T_{cav.} \sim 150^{\circ}\text{C}$) for ~48 hrs.
3. Conducting a H₂ gas glow discharge plasma cleaning (GDC) at $T_{cav.} \sim 200^{\circ}\text{C}$ for ~12hrs.
4. Coating a nucleation layer of Nb material (~10 atomic layers of Nb).
5. Annealing the layer at $T_{cav.} \sim 350^{\circ}\text{C}$ for 3hrs.
6. Coating (Thickening) Nb film till nominal 1.5 μm at $T_{cav.} \sim 350^{\circ}\text{C}$.
7. Stop heating the cavity, and start back-feeding O₂.
8. Take-out the cavity after cooling-down.

After this procedure was accomplished at AASC, the cavity was returned to Jefferson Lab. It was cleaned by high pressure water rinsing at a pressure of 180-200 PSI, then received the 1st round of cryogenic RF measurement. The coated niobium survived the 200 PSI HPR without visible change. The cavity then was high pressure water rinsed again at the standard pressure of 1200 PSI followed by a second cryogenic RF test. The coated niobium again survived the 1200 PSI HPR without visible change.

Following the 2nd round of RF test, LSF1-1 cavity went through a heat-treatment in a vacuum furnace of 450°C for 24 hrs at Jefferson Lab.

After the heat-treatment, LSF1-1 received another HPR at 1200 PSI; then LSF1-1 cavity went through the 3rd round of cryogenic RF measurement. The cavity was then cut into pieces by wire EDM in order to perform material analysis

Materials analysis, such as HiRox optical microscope, XRD Pole Figures, SEM-EDX, EBSD (in-plane view and cross-section view), TEM/STEM/EELS (sampling by FIB) were applied, in order to thoroughly reveal the microstructure of the Nb-Cu film in atomic, and nano/macro-scales. Some measurements have been finished, but others continue.

RESULTS AND DISCUSSION

Cryogenic RF Measurement

The first cryogenic RF test revealed that the input power coupler was too weakly coupled to the cavity. The uncertainty of the data was high, therefore the test was aborted. Nevertheless, the change in the resonance frequency as a result of the bath pressure change was measured to be -235 Hz/Torr.

During the 2nd cryogenic RF testing, two cernox sensors were attached to the cavity, one each at the upper and lower beam tube. A special cryogenic warm up procedure (from 4-10 K) was first applied, during which the resonance frequency and the loaded quality factor

were monitored automatically with a Labview program. This procedure allows determining the superconducting transition temperature T_c with two independent techniques. The measured T_c was found to be 9.33 K by both techniques. Figure 3 is the curve of the resonance frequency as a function of the cavity temperature.

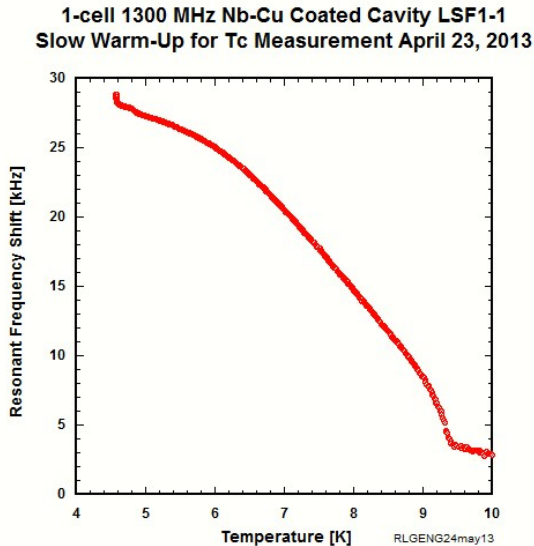


Figure 3: The resonance frequency of the cavity as a function of the cavity temperature.

After the T_c was experimentally determined, the cavity was slowly cooled down again to 2 K. The temperature difference between the upper and lower beam tube was measured to be around 20 mK. The cool down rate was controlled at 1.26 mK/sec while crossing T_c . The $Q(E_{acc})$ curve was then measured at 2K. The unloaded quality factor (Q_0) at low field was only 4×10^7 , followed by rapid decline as the gradient was raised. As the gradient was further raised, the rate of Q_0 decline was somehow much reduced. The dependence of Q_0 with temperature was also measured. By using the formula $R_s = G / Q_0$, where G is the geometry factor of the cavity, the surface resistance R_s can be calculated. Figure 4 shows the temperature dependence of the surface resistance. Clearly, the quality factor of the cavity is limited by the residual surface resistance, which is estimated to be on the order of $9 \mu\Omega$.

Finally, the cavity was heat treated in a vacuum furnace at 450 °C for 24 hours. The purpose of this procedure was to reduce the hydrogen that could have been added into the niobium coating layer or the copper substrate during the H_2 gas glow discharge plasma cleaning step. The coating survived the heat treatment, and no delamination of the niobium film was observed. The cavity was high pressure water rinsed again at 1200 PSI followed by cryogenic RF testing. This time, the cavity was cooled down through T_c in a standard fashion (i.e. no slow cool down). Typical cool down rate crossing T_c is estimated to be ~ 60 mK/sec. The cavity performance was improved as compared to that before the heat treatment with a low field Q_0 of 6×10^7 . However, the rapid decline of Q_0 with

gradient was still present. The highest gradient reached 1.7 MV/m, limited by cable heating.

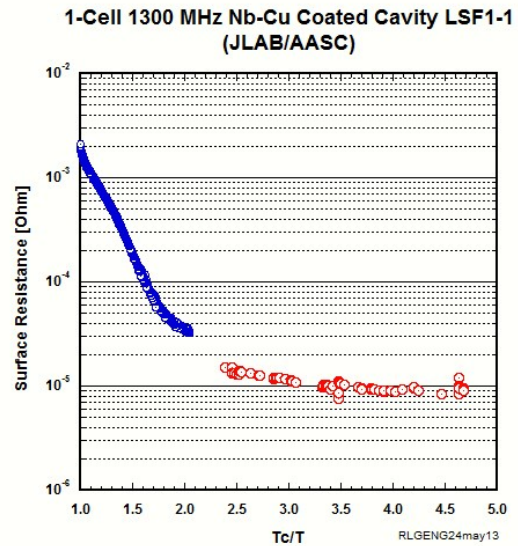


Figure 4: The temperature dependence of the surface resistance. The residual surface resistance is estimated to be $9 \mu\Omega$.

Materials Analysis to Reveal Microstructure of the LSF1-1 Nb-Cu Film

Visual Inspection

Inner (coating) surface of the LSF1-1 cavity appears smooth and uniform. It shows a specular, matte, grey and metallic hue of Nb material (Figure 5). The welding belt zone on the cavity equator appears no different than the other areas. Note the water-like stains in Figure 6 is a deposit left by the EDM. The pristine Nb-Cu surface was clear.



Figure 5: The pristine Nb-Cu surface of the LSF1-1 copper cavity. It appears a clear coating. The inner wall shows a specular, matte, grey and metallic hue of Nb material.

Next, the cavity was cut in half (Figure 6). HiRox optical microscope was applied to inspect its inner wall morphology, from tens toward a few thousand magnification.



Figure 6: A half-cavity piece cut from LSF1-1 Cavity.

Some visible uncoated copper areas associated with welding defects were observable in the equator region. They are up to a few millimeters in length, and a few hundred micrometers in width. There are only a few of them observable by eyes (<7 spots). Figure 7 shows a photo of such a defective area. Welding defects in the equator region were already observed before CBP. They were caused by insufficient melting and were not completely removed despite CBP. Please note these macroscopic defects are different from the microscopic cracks/blisters found under SEM analysis, which are in the scales of microns. We will discuss those later.

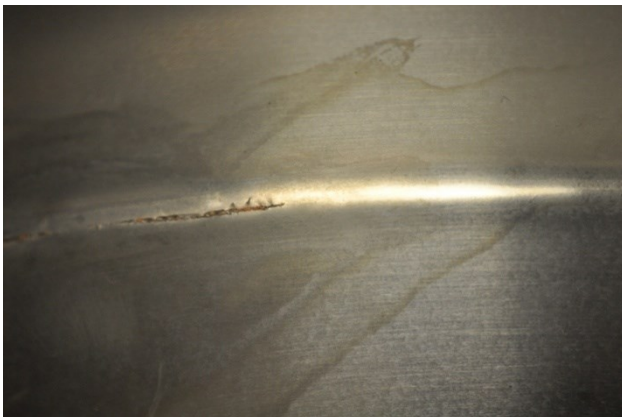


Figure 7: Some visible defects in the equator region showing uncoated copper. These defects are resulted from insufficient melting during electron beam welding. Deep welding defects are not totally removed by CBP.

One half-cavity (named “LSF1-1.2”) was further cut into 3 pieces, of which the centre one is an “Ω” shaped stripe 1 inch-wide (Figure 8, 9). That “Ω” shaped stripe was further cut into 8 small coupon samples of approximately one by one inch wide (Figure 10). All cutting services were conducted at Jefferson Lab’s machine shop via a wire EDM machine.

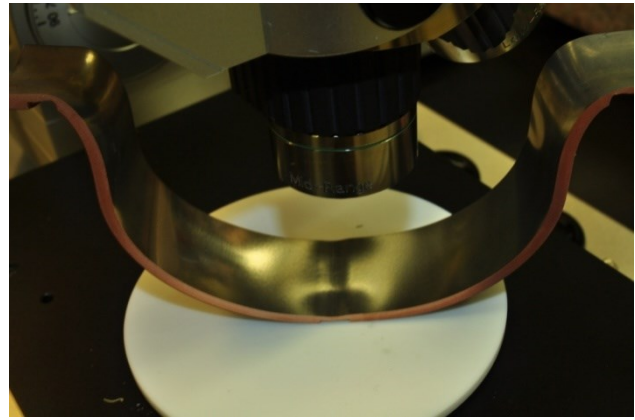


Figure 8: An “Ω”-shaped stripe of one inch wide was cut from a half cell.

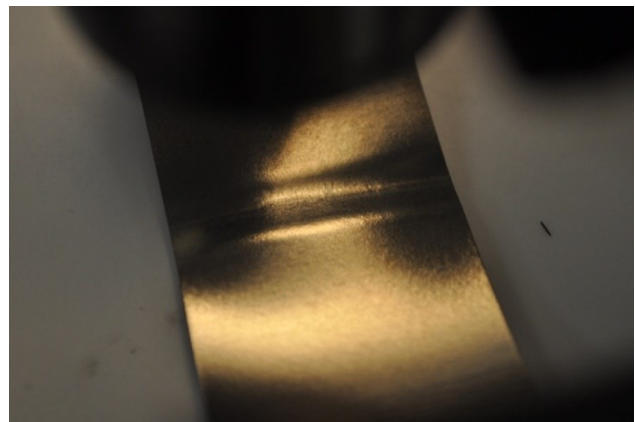


Figure 9: Coupon small sample “LSF1-1.2.4” was cut from the equator area. The welding belt zone appears no different from the other areas. The coatings seemed quite uniform.

After each EDM step, samples were cleaned by a standard UHV procedure. The final 8 small coupon samples were ultrasonic cleaned by detergent Micro. 90, then by methanol.



Figure 10: Set of 8 samples cut from the “Ω” shape of Figure 8. Coupon small sample “LSF1-1.2.4” (Left 4), has received SEM and XRD Pole Figure Measurement.

HiRox™ Optic Microscopy

HiRox Microscope examinations were conducted at the W&M surface analysis lab. The machine revealed surface topographic features at its max magnification of three thousand. Many spots on the cavity inner wall were surveyed along the “Ω” profile, touring from one iris area

(beampipe-cell junction), drum area, equator welding zone, finally toward the other side iris.

All images have some similar features: 1. Numerous round Nb macroparticles (a well-known by-product of unfiltered cathodic-arc-discharge deposition). 2. “Stripe-like” topography in macroscopic-scale, which is shaped by CBP media tumbling and friction. Figure 11 shows such defects.

In rare locations, a few peel-off areas were found. On those tiny defect areas, their top Nb films appeared being “skimmed off” by a fractural force. They exposed copper-like metallic hue. The spots were observable by a high magnification (of a few thousand. See Figure 12).

It’s unknown yet, whether they are caused by HPR stripping of weak coating areas. For instance, if debris/falling particles being introduced before coating, those areas have no Nb-Cu bonding. Under HPR, the loosely bound Nb material might be removed or torn off.

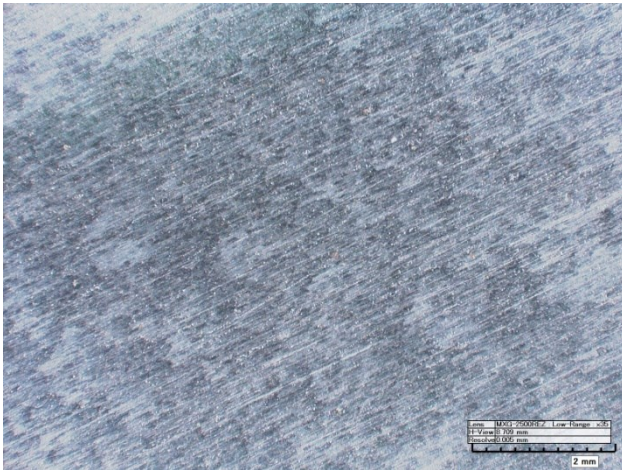


Figure 11: A low-mag micrograph of HiRox. “Stripe-like” topographic character in a macroscopic-scale, which feature is shaped by CBP media tumbling and friction.

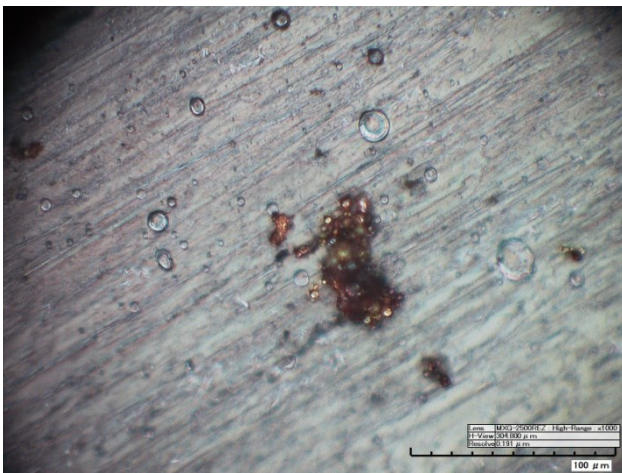


Figure 12: A high-mag micrograph of HiRox. Numerous round Nb macroparticles (a well-known by-product of unfiltered cathodic-arc-discharge deposition), and a few of peel-off areas.

On the EDM cutting plane (cross-section) of the welding zone, we observed two round pits on each side (Figure 13). The four bubble pits were far away from the inner or outer cavity wall (Figure 14). They are tens to a few hundred microns in diameter. Their round profiles and smooth appearance (Figure 15, 16) suggest that they are welding defects, being created by trapped gas bubbles during e-beam welding work.

In this sample, the four pits don’t impact the wall surface topography in this piece of sample. Nevertheless, in extreme cases, if bubble pits were close to the wall surface, a CBP finishing might create reveal a deep pit on the cavity wall.

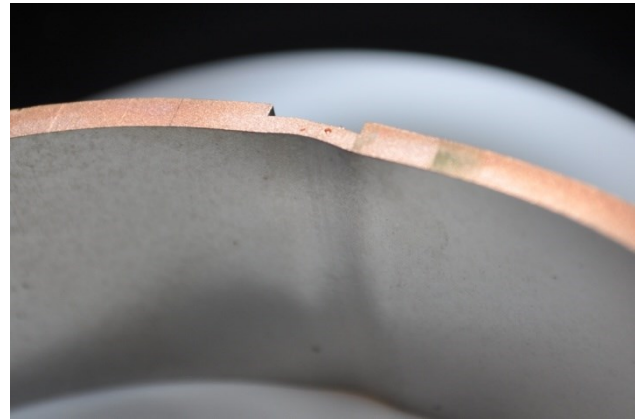


Figure 13: Welding bubbles are visible on EDM cutting planes.

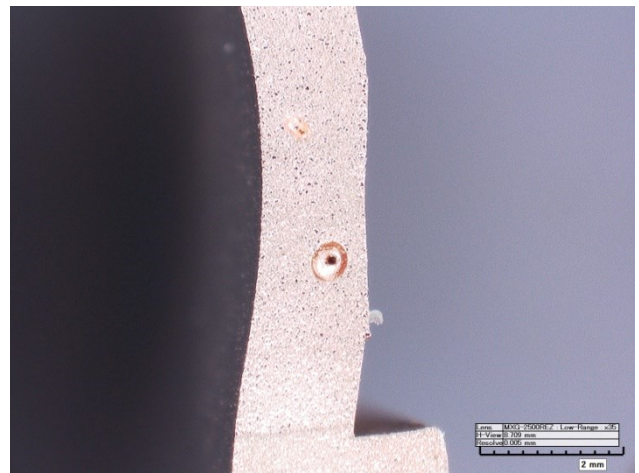


Figure 14: A low-mag micrograph of HiRox. The pits are far away from inner or outer walls.

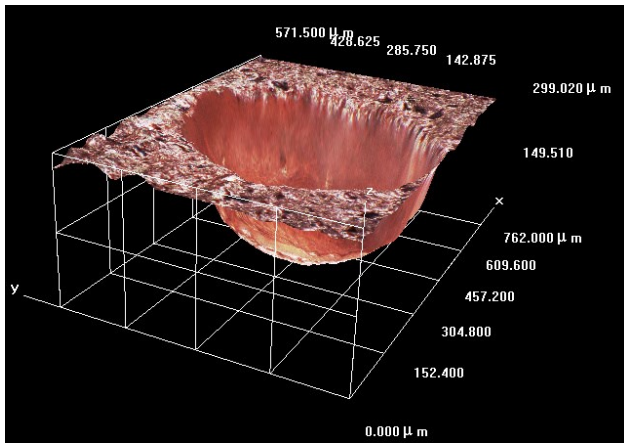


Figure 15: A view of HiRox 3D Imaging on a bubble pit.

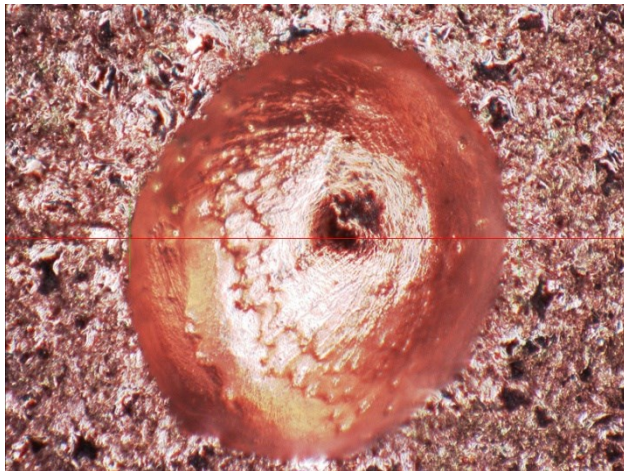


Figure 16: The round up and shining appearance of bubble pits imply they are defects of welding work.

SEM Imaging

Coupon small samples “LSF1-1.2.2” and “LSF1-1.2.4” were surveyed on different instruments.

SEM work on sample “LSF1-1.2.4” was conducted at the W&M Surface Lab via an Hitachi 4700 Field Emission high resolution SEM/EDX. This SEM could discern topographic contrast from magnification of 30X to 50,000X (in nanometer scale).

Sample “LSF1-1.2.4” was located at the equator zone, the welding belt of a few millimetres wide running across the middle of the sample. Both welding zone and non-welding zones were scanned by SEM.

Under SEM (up from low mag. 100X), the stripe-like CBP finishing morphology is still observable (Figure 17).

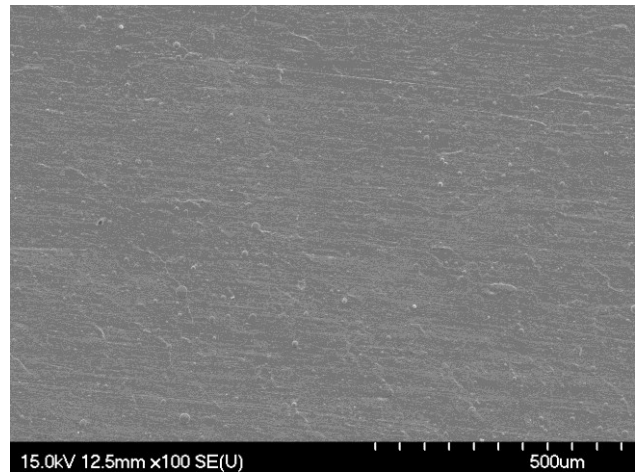


Figure 17: SEM micrograph of a low magnification imaging (100X) on coupon small sample “LSF1-1.2.4”. Spot on a welding zone, whose topography is not different from a non-welding zone.

Unsurprisingly, macroparticles of CED cathodic arc discharge are visible everywhere (Figure 18). Nevertheless, under high resolution high magnification imaging, microscopic cracks/blisters were also found everywhere (Figure 19). They are typically from tens to hundreds of microns long, hundreds or tens of nanometers wide at their maximum openings (Figure 20).

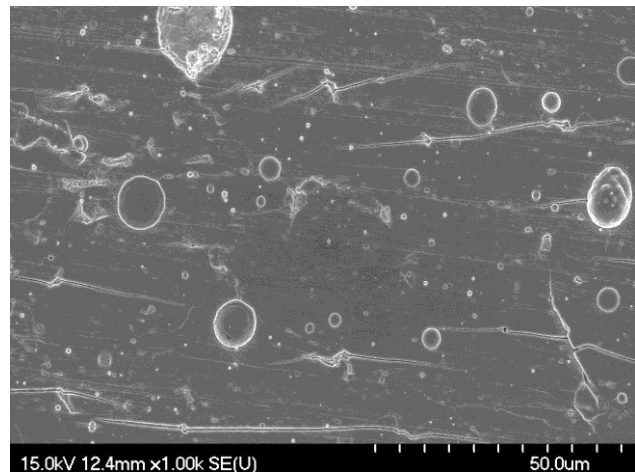


Figure 18: SEM micrograph of sample “LSF1-1.2.4” (mag. 1000X) showing CED arc-discharge particles and microscopic cracks/blisters .

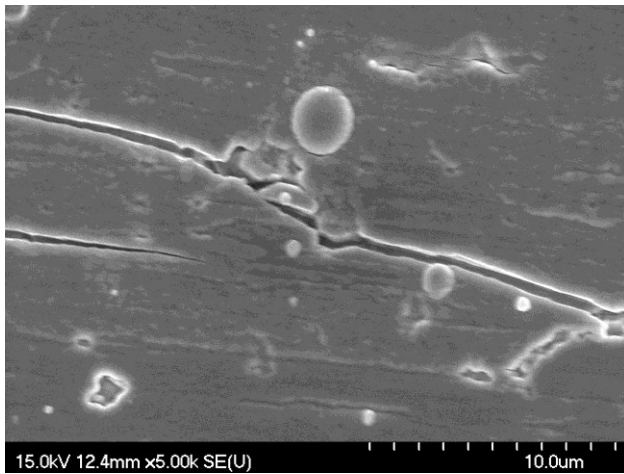


Figure 19: SEM micrograph (mag. 5000X). Microscopic cracks/blisters are typically from tens to hundreds of microns long.

It's not known yet, if the cracks were caused by thermal stress induced film delaminating during coating procedure, or in the oven heat-treatment post the 2nd RF measurement. Film cracking or delamination tensile/compression stress is a well known phenomenon in film deposition technology. Please note these omnipresent microscopic cracks are different than the aforementioned few macroscopic cracks in the weld zone.

SEM work on sample "LSF1-1.2.2" was conducted at the Applied Superconductivity Center at the National High Magnetic Field Laboratory, at Florida State University, via a Zeiss 1540 EsB Cross Beam Scanning Electron Microscope. This is a state-of-the-art dual beam field emission Scanning Electron Microscope (SEM) with an ultimate resolution of 1 nanometer. It is fully computer controlled with multi-resolution digital image capture. It is equipped with a low-energy capable Focused Ion Beam (FIB) column, which allows for live-imaging of samples at high magnification, while simultaneously machining with 5 nm precision using a stream of Ga ions.

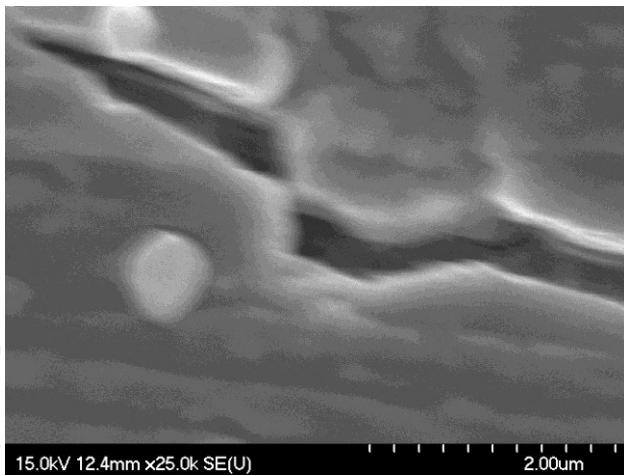


Figure 20: SEM micrograph (mag. 25,000X) of a crack. Microscopic cracks/blisters are hundreds or tens of nanometers wide at their max openings.

Sample "LSF1-1.2.2" was located near the iris zone of the cavity. Because the EsB machine has superior resolution, rough surface morphology by CBP finishing is more apparent (Figure 21). By FIBing and viewing the cross-section of the Nb-Cu film interface, SEM indicates the thickness of the film is quite uniform. Its thickness is about 700 nm (Figure 22). Preliminary EBSD survey on this sample doesn't see grain structure. This suggests either the grain sizes are less than 50nm (the limit of EBSD resolution) and/or the grains have large stress/strain. This demonstrates that the Nb-Cu film is by no means an epitaxy film.

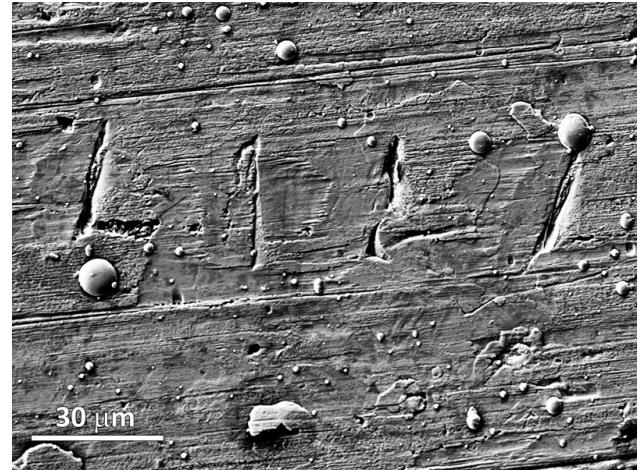


Figure 21: SEM micrograph of Sample "LSF1-1.2.2". Courtesy of NHMFL-ASC, a work by Zu-Hwan Sung.

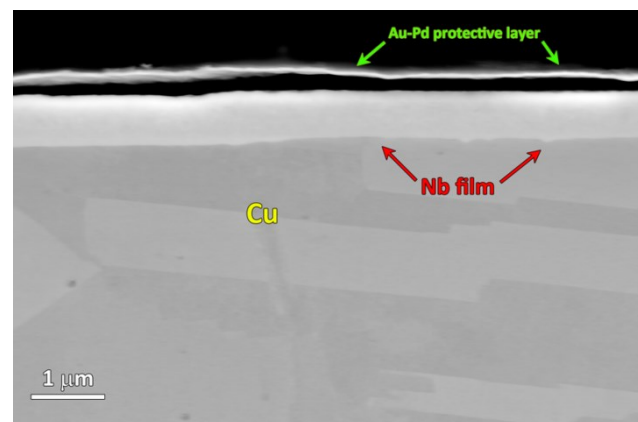


Figure 22: SEM micrograph of Sample "LSF1-1.2.2". The cross-section view of Nb-Cu film interface. Courtesy of NHMFL-ASC, a work by Zu-Hwan Sung.

To observe Nb-Cu interface morphology, the cross-sectional plane of the sample was etched with 50% diluted BCP solution for 20-30sec, it shows fibrous structure of Nb film, a CBP-finished buffer layer, and an underlying crystalline copper substrate in different layers (Figure 23).

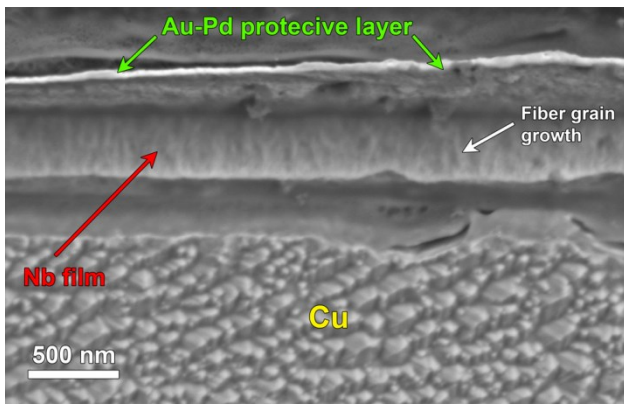


Figure 23: Cross-section view of Nb-Cu film interface, after a BCP etching. Courtesy of NHMFL-ASC, a work by Zu-Hwan Sung.

Texture Measurement by XRD Pole Figure

XRD measurement was conducted at Norfolk State University. The same coupon small sample, “LSF1-1.2.4” was surveyed. The X-ray survey area was on a non-welding zone, which plateau is very flat and suitable for XRD reflection geometry. A survey in Bragg-Brentano mode ($\theta/2\theta$) proved that the Nb film has a classic polycrystalline structure. There are a variety of $\{hkl\}$ crystal planes (grain orientations) parallel to the sample surface (Figure 24).

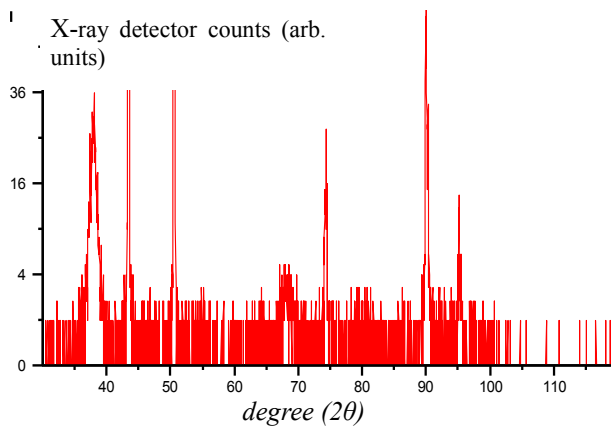


Figure 24: XRD in Bragg-Brentano mode ($\theta/2\theta$ scan) on coupon small sample, “LSF1-1.2.4”.

The XRD pole figure of Nb{110} planes (Figure 25), shows an obvious broad centre peak, and a diffusive “ring” at orbital $\psi = 60^\circ$. This ring pattern indicates the Nb film has a preferential orientation: a Nb{110} *in-plane* fibrous texture. This means, a majority of the Nb grains expose one {110} plane parallel to the cavity wall surface, while the grains have different azimuthal orientations *off-plane*. The off-plane orientations have a uniform distribution; therefore, the ring texture pattern is quite even. Such texture implies that the Nb film was growing in a fibrous mode or fibrous microstructure, rather than the Nb-Cu epitaxial mode. This is one preliminary evidence of success in implementing a multi-layer structure by our coating procedure.

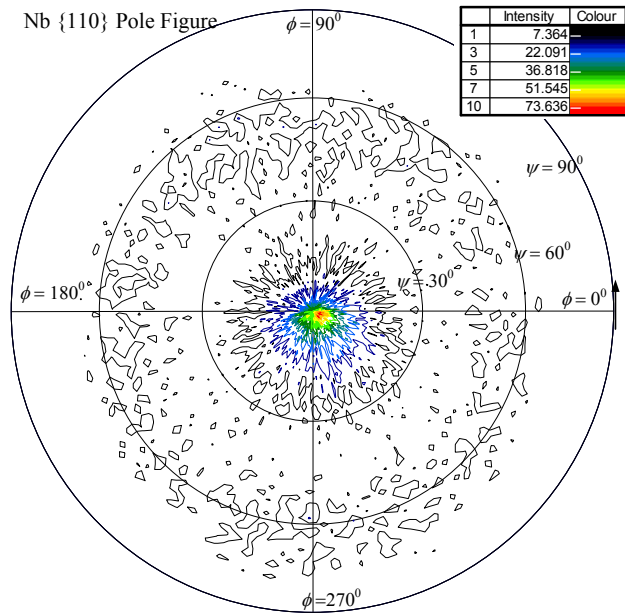


Figure 25: Experimental XRD pole figure of the coupon small sample, “LSF1-1.2.4”. The Nb{110} pole figure shows an obvious broad centre peak, and a diffusive “ring” at orbital $\psi = 60^\circ$. This ring pattern implies the Nb film has a fibrous grain microstructure.

SUMMARY

Nb film growth on a single cell Cu cavity was attempted using a novel procedure. The cavity was cryogenically tested several times after various surface cleaning and cavity heat treatment procedures. Clear superconducting transition was measured. The niobium coating survived repeated high pressure water rinsing and temperature cycling including cryogenic cycling and high temperature cycling. The quality factor of the cavity was dominated by the residual resistance. Uncoated copper associated with welding defects in the equator is a known source for the high residual resistance. From the measurement data, we estimate a surface resistance of the coated niobium on the same order as that of standard bulk niobium. Detailed examination of the surface reveals numerous features that will feedback on process improvement. Preliminary materials analysis by EBSD and XRD Pole Figures indicate the film has a fibrous and Nb{110} *in-plane* texture. Such a fibrous growth mode supports our conceptual design on microstructure. More materials analysis, such as HRTEM/STEM/EELS are required to fully understand the film’s growth mode and its microstructure evolution. Future film coated-cavity work will be carried out with copper cavities free from welding defects in equator region. Further tests will be done to assess the possibility of hydrogen embedment due to hydrogen glow discharge cleaning.

ACKNOWLEDGMENTS

We sincerely appreciate our long term collaborators at Alameda Applied Sciences Corporation (AASC), Drs. Mahadevan Krishnan and Colt James, for supporting this research by their novel thin film deposition technology. We also acknowledge the Surface Analysis Lab of College of William & Mary at ARC for their support on the HiRox and SEM measurements. We would like to acknowledge Dr. Charles Reece at Jefferson Lab for his sustained support of this activity. Special thanks to the kindly and timely support of Drs. Zu-Hwan Sung and P.J Lee of NHMFL-ASC at FSU for materials analysis work. This manuscript has been authored by Jefferson Science Associates, LLC under U.S. DOE Contract No. DE-AC05-06OR23177. The U.S. Government retains a non-exclusive, paid-up, irrevocable, world-wide license to publish or reproduce this manuscript for U.S. Government purposes.

REFERENCES

- [1] A. D. Palczewski, et al., These preceding TUIOB01, SRF2013, Paris France (2013); CBP recipe and removal, et al. A. D. Palczewski, et al., These preceding, TUP062, SRF 2013. Paris, France. (2013).
- [2] X. Zhao, et al., Journal of Vacuum Science & Technology A 27 (4), 620-625 (2009); M Krishnan, et al, Supercond. Sci. Technol. (24), 115002 (2011); X. Zhao, et al., Journal Applied Physics 110, 033523 (2011) and J. Appl. Phys. 112, 016102 (2012); M. Krishnan, et al., Physical Review Special Topics - Accelerators and Beams., 15, 032001 (2012).